Bloch–Zener Oscillations in Graphene and Topological Insulators

Viktor Krueckl and Klaus Richter

Institut für Theoretische Physik, Universität Regensburg, D-93040 Regensburg, Germany
(Dated: September 27, 2011)

We show that superlattices based on zero-gap semiconductors such as graphene and mercury telluride exhibit characteristic Bloch–Zener oscillations that emerge from the coherent superposition of Bloch oscillations and multiple Zener tunneling between the electron and hole branch. We demonstrate this mechanism by means of wave packet dynamics in various spatially periodically modulated nanoribbons subject to an external bias field. The associated Bloch frequencies exhibit a peculiar periodic bias dependence which we explain within a two-band model. Supported by extensive numerical transport calculations, we show that this effect gives rise to distinct current oscillations observable in the *I-V* characteristics of graphene and mercury telluride superlattices.

Bloch oscillations, the periodic motion of particles in a superlattice subject to a constant external field, represent a fundamental phenomenon in transport through periodic potentials. Predicted already in the early days of quantum mechanics [1], Bloch oscillations have been observed in various fields of physics, ranging from earlier experiments in semiconductor superlattices [2] via cold atoms in optical lattices [3] to classical optical [4] and acoustic [5] waves. While many aspects of conventional Bloch oscillations can be explained by a single band description, particularly interesting effects arise in the case of two coupled minibands [6] energetically seprated from further bands. Then partial Zener tunneling at avoided crossings of the two minibands can lead to a coherent superposition of Bloch oscillations [7], *i.e.* to a splitting, followed by as subsequent recombination of a Bloch oscillating wave packet. This gives rise to a variety of Rabi-type interference phenomena, in particular double-periodic motions coined Bloch–Zener (BZ) oscillations [8]. Signatures of this effect have already been detected in the THz emission of AlGaAs superlattices [9], and even the population dynamics has been measured recently for light [10] and atomic matter waves [11] in especially tailored binary lattices.

However, materials with a linear Dirac spectrum [12] should naturally provide the effect, since only a small gap is opened by a spatially periodic modulation allowing for Zener tunneling between electron and hole states. Such materials are now at hand with the discovery of graphene [13] and the advent of topological insulators [14] first realized in two-dimensional mercury telluride (HgTe) heterostructures [15]. Interesting phenomena for graphene superstructures have already been theoretically predicted like the formation of extra Dirac cones [16] and the appearance of a negative differential conductance [17]. Furthermore recent experiments have realized graphene superlattices with periodicities down to a few nm [18].

This raises the question for the existence of Bloch oscillations and their possible peculiarities in graphene and topological insulator superlattices that we address in this manuscript [19]. We show that besides conventional Bloch oscillations, multiple Zener tunneling between the coupled electron and hole branches leads to distinct BZ oscillations that appear to be naturally present in superlattices made of systems with Dirac-like dispersion. We demonstrate the influence of these tunneling events on the wave packet motion in biased graphene nanoribbons and explain the effect by a two-band model. Subsequently, we present how transport through graphene and mercury teluride is affected by such BZ oscillations and suggest possible setups for an experimental detection.

We start with the dynamics of a wave packet undergoing Bloch oscillations on a graphene nanoribbon with a periodic mass potential $M(x) = M_0 \sin(2\pi x/a)$ and a linear drift potential $V(x) = -eE_D x$ as sketched in Fig. 1(a). To this end we model the electronic structure of graphene by a conventional tight-binding Hamiltonian [21]

$$H_{\text{tb}} = \sum_{\langle i\ j\rangle,\beta} t\ c^{\dagger}_{i,-\beta}c_{j,\beta} + V\ c^{\dagger}_{i,\beta}c_{i,\beta} + M\ \beta\ c^{\dagger}_{i,\beta}c_{i,\beta} \quad (1)$$

where $\langle i\ j\rangle$ denotes neighbouring unit cells and $\beta = \pm 1$ the sublattice degree of freedom. Based on the transversal eigenstates of the armchair terminated nanoribbon, we create an initial wave packet localized in one band with a Gaussian envelope in longitudinal direction covering several periods a of the periodic potential. Due to this extent, the wave packet is also localized in momentum space with a distinct average momentum in x-direction. We calculate the time evolution of the wave packet by a Chebechev propagation algorithm [22] and extract the center-of-mass (COM) motion. In presence of the drift field E_D the wave packet starts to accelerate and, given the periodicity of its average momentum $k(t)$, we get a sawtooth behavior of $k(t)$ known as Bloch oscillations. Moreover, as shown in Fig. 1(b), a single trajectory of the wave packet exhibits a beating pattern on top of regular Bloch oscillations which suggests that more bands are involved in the time evolution. This behavior is also
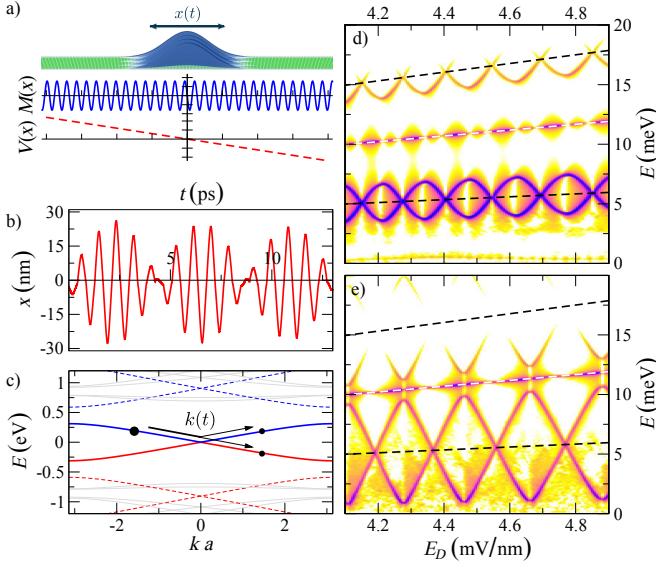
FIG. 1. (*Color online*) Bloch oscillations in a graphene nanoribbon. a) Sketch of a Gaussian wave packet in presence of a periodic mass potential $M(x) = M_0 \sin(2\pi x/a)$ and drift potential $V(x) = -eE_D x$. b) COM motion of the wave packet showing a beating pattern ($E_D = 4.025$ mV/nm, nanoribbon width $W = 10\ a_0$, $a = 10\sqrt{3}\ a_0$, $M_0 = 0.1\ t$). c) Bandstructure of the superlattice with small avoided crossing at $k = 0$. Thick and dashed lines show the first and second Bloch band from the metallic armchair mode; gray lines higher modes. d,e) Frequency spectra $E = \hbar\omega$ from the COM motion of a wave packet for varying drift potential E_D for (d) moderate ($M_0 = 0.1t$) and (e) stronger ($M_0 = 0.2t$) periodic potential. Dark colors represent strong intensities. The dashed lines correspond to $\{1/2, 1, 3/2\}$ times the conventional Bloch frequency.

deducible from the mini-band structure of the superlattice as shown in Fig. 1(c). A state initially starting on the electronic branch (large bullet in Fig. 1(c)) can tunnel into the hole branch through a small avoided crossing at $k(t) = 0$. To study this dynamics we perform a frequency analysis of the COM motion for different E_D. The Fourier amplitudes of the dominant frequency contributions are visualized by dark colors in Fig. 1(d,e). Besides the conventional Bloch frequency (white dashed line), the resulting spectrum shows a pronounced interweaving pattern around half of this frequency (black dashed line). A stronger periodic potential, and thereby an increased gap between electron and hole branch, leads to a rhombic structure as shown in Fig. 1(e). These periodic features in the frequency spectrum arise from the interplay between Bloch oscillations and splitting the wave packet into (subsequently interfering) electron and hole branches at $k(t) = 0$ (see Fig. 1(c) and Supplemental Material [23]).

In the following we quantitatively explain these characteristic BZ features using a periodically modulated one-
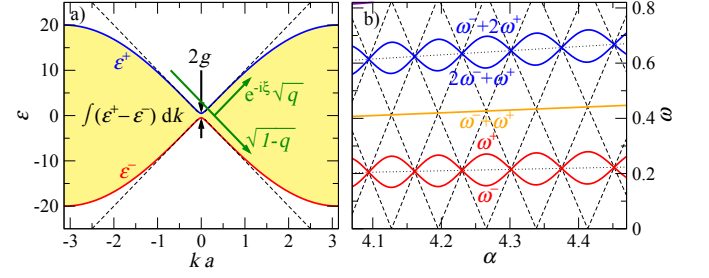

FIG. 2. (*Color online*) a) Bandstructure of the Dirac model Hamiltonian (2) for $v = 1$, $\hbar = 1$, $a = 1/10$, $g = 1/2$. b) Frequency spectrum of the Bloch oscillations for different drift accelerations $\alpha = eE_D/\hbar$. Solid lines show the frequencies $n\omega^+ + m\omega^-$ given by Eq. (7), dotted (dashed) lines the strong (weak) tunneling limit.

dimensional Dirac model Hamiltonian,

$$H(t) = \frac{2\hbar v}{a} \sin\left(\frac{ak(t)}{2}\right)\sigma_z + g\,\sigma_x. \qquad (2)$$

Here a is the period, v is the Fermi velocity and g the energy gap between the electron and the hole states. The resulting bandstructure is given by

$$\epsilon^{\pm}(t) = \pm\sqrt{g^2 + 2(\hbar v/a)^2\left[1 - \cos(ak)\right]} \qquad (3)$$

as shown in Fig. 2(a) [to be compared to full tight-binding result of Fig. 1(c)]. A drift field E_D enters the equations of motion for the quasi-momentum $k(t)$ as $\hbar\,\partial_t k(t) = eE_D$ leading to a time evolution of $k(t) = \alpha t$ linear in t where $\alpha = eE_D/\hbar$. Conventional Bloch oscillations with frequency $\omega_B = \alpha a$ arise from the periodicity of $k(t)$ in momentum space in the interval $[-\frac{\pi}{a}, \frac{\pi}{a}]$. The phase ϕ between the two branches accumulated during one oscillation is given by a free propagation and thus $\phi = \mathcal{A}(eE_D)^{-1} \approx \frac{16v}{a^2\alpha}$ with $\mathcal{A} = \int_{-\pi/a}^{\pi/a}(\epsilon^+ - \epsilon^-)\mathrm{d}k$ the area in momentum space as depicted in Fig. 2(a). This free propagation can be expressed by the matrix

$$U_0 = \begin{pmatrix} e^{i\phi/2} & 0 \\ 0 & e^{-i\phi/2} \end{pmatrix}. \qquad (4)$$

Additional to conventional Bloch oscillations on either branch, there is a strong periodic tunneling between the electron and the hole states close to the anti-crossing at $k = 0$. There, the Hamiltonian (2) can be linearized [dashed lines in Fig. 2(a)], leading to a typical Landau–Zener tunneling problem [24]:

$$H_{\mathrm{LZ}} = \begin{pmatrix} \hbar v\ \alpha t & g \\ g & -\hbar v\ \alpha t \end{pmatrix}. \qquad (5)$$

Scattering between the different branches is described by

$$S_0 = \begin{pmatrix} e^{-i\xi}\sqrt{q} & \sqrt{1-q} \\ \sqrt{1-q} & -e^{i\xi}\sqrt{q} \end{pmatrix} \qquad (6)$$

with the tunneling rate $q = 1 - e^{-2\pi\delta}$, $\delta = \frac{g^2}{2\hbar^2 v\alpha}$, and $\xi = \frac{\pi}{4} + \arg(1-i\delta) + \delta(\log\delta - 1)$ is an additional tunneling phase. From this we can deduce the scattering matrix for one Bloch oscillation as $S = U_0 S_0$. The periodicity of the scattering eigenstates, given by the argument of their eigenphases, leads to two new Bloch frequencies

$$\omega^{\pm} = \frac{\alpha a}{\pi} \arccos\left[\pm\sqrt{q}\sin(\phi/2 - \xi)\right]. \quad (7)$$

Unlike standard Bloch oscillations these frequencies do not simply depend linearly on the drift strength α, but show a rapid interweaving pattern, as shown in Fig. 2(b), owing to coherences from combined dynamics on the hole and electron branch. For strong coupling, the tunneling rate $q \to 0$ leads to a frequency $\omega^{\pm} \to \omega_B/2$ [dotted line in Fig. 2(b)], since for every Bloch cycle the states tunnel completely between the two branches in momentum space and hence the complete cycle in position space is twice as long. In the opposite, weak coupling limit $\omega^{\pm} \to a\alpha[1/2 \pm (\phi/2 - \xi)/\pi]$ mod 1 leading to a rhombic frequency pattern shown as dashed lines in Fig. 2(b). For intermediate tunneling rates the frequencies show a smooth transition between these limiting cases and are in very good agreement with the numerically calculated spectra of Fig. 1(d,e).

In the following, we consider charge transport through graphene nanoribbon superlattices and demonstrate that BZ oscillations lead to clear-cut features in the I-V characteristics. To this end we model a graphene nanoribbon of width W and length L by the tight-binding Hamiltoninan of Eq. (1) now with a periodic electrostatic potential $V_0 \sin(2\pi x/a)$ leading to a superlattice minibandstructure as shown in the inset of Fig. 3(a). A small constant mass term $M(x) = M_0$ is additionally considered which opens up a gap commonly present in experiments on graphene nanoribbons [25]. We assume a linear potential drop $eV_{SD}x/L$ due to the source-drain voltage V_{SD} between the graphene leads at $x = \pm L/2$. The current is calculated by means of the Landauer-Büttiker formalism [26],

$$I(V_{SD}) = \frac{2e}{h} \int_{-\infty}^{\infty} T(E, V_{SD})[f^+(E) - f^-(E)]dE, \quad (8)$$

with $f^{\pm}(E) = \{1 + \exp[(E \mp V_{SD}/2)/k_B T]\}^{-1}$.

As shown in Fig. 3, the current through the nanoribbon is governed by a conventional increase with the bias window for small V_{SD}, followed by a region of negative differential conductance typical for superlattices. At higher bias, $V_{SD} > 0.3$ V, we observe the emergence of distinct current oscillations that get more pronounced with increasing gap size, see Fig 3(b). Due to the bias potential the particles traversing the superlattice must change their electron-hole character. However, states performing BZ oscillations exhibit transitions between the two carrier types only for certain $V_{SD} = eE_D L$ if the phase
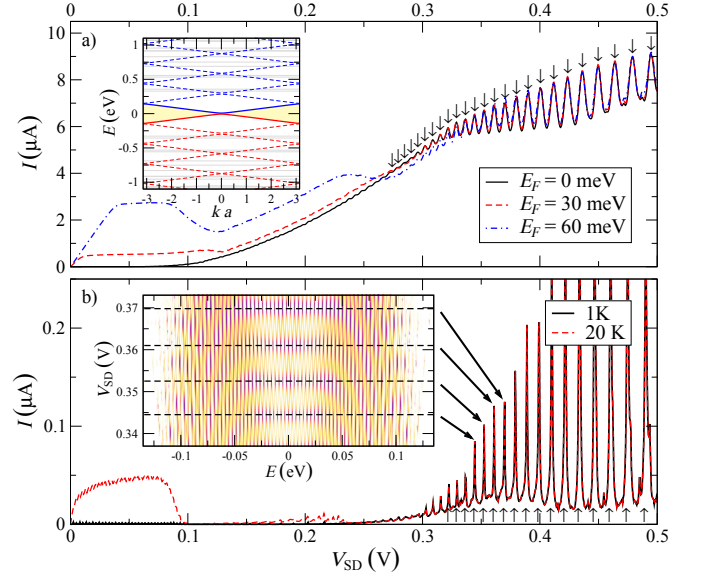

FIG. 3. (*Color online*) Current-voltage characteristics for graphene nanoribbon superlattices ($L = 3000\sqrt{3}a_0$, $W = 10a_0$, $a = 30\sqrt{3}a_0$, $V_0 = 500$ meV) for (a) different Fermi energies ($M_0 = 20$meV, $T = 20$K) and (b) different temperatures ($M_0 = 50$meV, $E_F = 0$) showing signatures of Bloch–Zener oscillations at higher bias. Arrows mark expected peak positions from phase condition (9). Upper inset: Bandstructure (for $M_0 = 20$meV), lower inset: Transmission map $T(E, V_{SD})$ used in Eq. (8) to get the current of panel (b); dark colors represent high transmissions.

[see Eq. (4)] fulfills

$$\phi = \frac{\mathcal{A}L}{V_{SD}} = 2(n\pi + \xi) + \pi \qquad (n \in \mathbb{N}) \quad (9)$$

as shown in the Supplemental Material [23]. In consequence the current is strongly enhanced whenever ϕ fulfills this condition. As shown in Fig. 3(a,b) the current peaks calculated by Eq. (8) perfectly coincide with the expected voltages (marked by vertical arrows) deduced by extracting the area $\mathcal{A}$ in momentum space from the minibandes around the Fermi energy shown as shaded area in the inset of Fig. 3(a). Vice versa, the experimental observation of BZ peaks in the I-V characteristics would allow for 'measuring' the miniband structure.

A closer look at the transmission values $T(E, V_{SD})$ [see inset Fig. 3(b)] reveals a rhombic structure which features pronounced transmission maxima piled up for the particular values of V_{SD} (dashed lines) in accordance with Eq. (9). Since these maxima are present for various energies in the conductance window, the resulting current is fairly independent of the exact Fermi energy [see Fig. 3(a)] and temperature [see Fig. 3(b)].

The whole frequency spectrum of the BZ oscillations can be monitored, if the current is measured in presence of a tunable laser field. We present corresponding Floquet transport calculations for graphene nanoribbons in
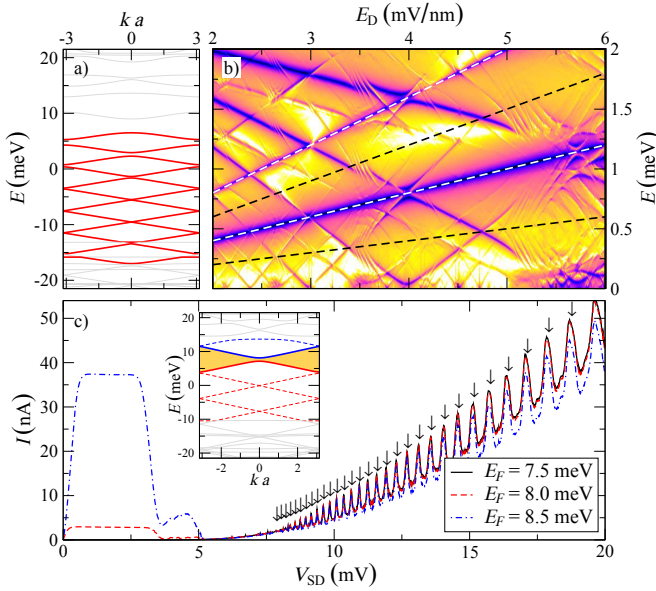
FIG. 4. (*Color online*) Bloch and Bloch–Zener oscillations in spatially modulated two-dimensional HgTe nanoribbons. a) Bandstructure for a HgTe nanoribbon with periodically modulated width $W(x)$ ranging from $W_0 = 300$ nm to $W_1 = 50$ nm and periodicity $a = 200$ nm [23]. b) Bloch frequency spectrum $E = \hbar\omega$ of the wave packet COM motion as a function of drift field E_D. c) I-V_{SD} characteristics of a nanoribbon with constant width $W = 150$ nm and electrostatic modulation $V(x) = V_0 \sin(2\pi x/a)$. Small vertical arrows mark expected maxima from Eq. (9). Inset: corresponding minibandstructure.

the Supplemental Material [23] which show a strongly increased transmission when laser and BZ frequencies are in resonance.

A different setup featuring BZ oscillations can be created from a strip etched out of the two-dimensional topological insulator based on mercury teluride (HgTe) [15]. Periodically modulating the width of this strip leads to a cyclic change in the mass of an effective one-dimensional model [27]. The numerically obtained resulting miniband structure, shown in Fig. 4(a), exhibits various Landau-Zener anticrossings within the bulk bandgap of HgTe which suggest BZ oscillations. In order to study the electron dynamics we calculate the COM motion of Gaussian shaped edge-state wave packets. Initially, the wave packet is localized on one edge and the direction of motion is determined by its spin. The array of multiple constrictions allows for tunneling to the opposite edge, leading to an inversion of the motion and Bloch oscillations in the COM motion. As shown in Fig. 4(b), the resulting frequency spectrum features the expected rhombic pattern inbetween the frequencies of the conventional Bloch oscillations (white dashed lines). Compared to the graphene system [see Fig. 1(e)] we observe more complicated, superimposed structures due to the whole sequence of multiple anticrossings in the band structure.

As for graphene we further study the transport properties of HgTe strips of constant width and a periodically modulated electrostatic potential resulting in a supercell bandstructure shown in the inset of Fig. 4(c). We chose the Fermi energy close to the band crossing of the topological edge states and calculate the current using Eq. (8). Besides a strong negative-differential conductance at lower bias we get BZ oscillations for $V_{SD} > 9$ mV as shown in Fig. 4(c). Similar to the calculations for the graphene superlattice the oscillations are independent of the exact choice of the Fermi level. The peak positions are in good accordance with the expected series of drift voltages, Eq. (9), marked by arrows in Fig. 4(c) where $\mathcal{A}$ is extracted from the bands around the Fermi energy shown as shaded area in the inset.

In this manuscript we show that Bloch–Zener oscillations appear naturally in superlattices made of materials with a Dirac-like spectrum highlighting interference between electron and hole states. The characteristics of those oscillations are explained by a one-dimensional model Hamiltonian and numerically confirmed for realistic setups by means of wave packet simulations and transport calculations. Furthermore we suggest transport measurements through graphene nanoribbons and HgTe strips as promising experimental setups that feature Bloch–Zener oscillations leading to sequences of pronounced current peaks.

[1] F. Bloch, Z. Phys. A **52**, 555 (1929); C. Zener, Proc. R. Soc. Lond. A **145**, 523 (1934).

[2] J. Feldmann *et al.*, Phys. Rev. B **46**, 7252 (1992); K. Leo *et al.*, Solid State Communications **84**, 943 (1992); C. Waschke *et al.*, Phys. Rev. Lett. **70**, 3319 (1993).

[3] M. Ben Dahan *et al.*, Phys. Rev. Lett. **76**, 4508 (1996); S. Wilkinson *et al.*, Phys. Rev. Lett. **76**, 4512 (1996).

[4] T. Pertsch *et al.*, Phys. Rev. Lett. **83**, 4752 (1999); R. Morandotti *et al.*, Phys. Rev. Lett. **83**, 4756 (1999).

[5] H. Sanchis-Alepuz, Y. Kosevich, and J. Sánchez-Dehesa, Phys. Rev. Lett. **98**, 134301 (2007).

[6] H. Fukuyama, R. Bari, and H. Fogedby, Phys. Rev. B **8**, 5579 (1973).

[7] J. Rotvig, A.-P. Jauho, and H. Smith, Phys. Rev. Lett. **74**, 1831 (1995); D. Hone and X.-G. Zhao, Phys. Rev. B **53**, 4834 (1996).

[8] B. Breid, D. Witthaut, and H. Korsch, New J. Phys. **8**, 110 (2006); New J. Phys. **9**, 62 (2007); P. Abumov and D. W. L. Sprung, Phys. Rev. B **75**, 165421 (2007).

[9] Y. Shimada, N. Sekine, and K. Hirakawa, Appl. Phys. Lett. **84**, 4926 (2004).

[10] F. Dreisow *et al.*, Phys. Rev. Lett. **102**, 076802 (2009).

[11] S. Kling, T. Salger, C. Grossert, and M. Weitz, Phys.

Rev. Lett. **105**, 215301 (2010).

[12] P. Wallace, Phys. Rev. **71**, 622 (1947).

[13] K. Novoselov *et al.*, Science **306**, 666 (2004); Y. Zhang, Y.-W. Tan, H. Stormer, and P. Kim, Nature **438**, 201 (2005).

[14] C. Kane and E. Mele, Phys. Rev. Lett. **95**, 226801 (2005); Phys. Rev. Lett. **95**, 146802 (2005); B. Bernevig, T. Hughes, and S.-C. Zhang, Science **314**, 1757 (2006);

[15] M. König *et al.*, Science **318**, 766 (2007); A. Roth *et al.*, Science **325**, 294 (2009).

[16] C.-H. Park *et al.*, Nat. Phys. **4**, 213 (2008); L. Brey and H. Fertig, Phys. Rev. Lett. **103**, 046809 (2009); M. Barbier, P. Vasilopoulos, and F. Peeters, Phys. Rev. B **81**, 075438 (2010).

[17] G. Ferreira, M. Leuenberger, D. Loss, and J. Egues, arXiv 1105.4850v1 (2011).

[18] J. Meyer, C. Girit, M. Crommie, and A. Zettl, Appl. Phys. Lett. **92**, 123110 (2008).

[19] We are not aware of work on graphene-based Bloch oscillations beside Ref. [20] using the standard semiclassical approach adapted to a linear dispersion.

[20] D. Dragoman and M. Dragoman, Appl. Phys. Lett. **93**, 103105 (2008).

[21] K. Nakada, M. Fujita, G. Dresselhaus, and M. Dresselhaus, Phys. Rev. B **54**, 17954 (1996).

[22] V. Krueckl and T. Kramer, New J. Phys. **11**, 093010 (2009).

[23] See Supplemental Material at ??? for a video of Bloch–Zener oscillations on a graphene superlattice, electron-hole polarization properties of the model Hamiltonian, laser assisted transport and details of the model used for HgTe superlattices.

[24] L. D. Landau, Phys. Z. Sowjetunion **2**, 46 (1932); C. Zener, Proc. R. Soc. Lond. A **137**, 696 (1932); E. C. G. Stueckelberg, Helv. Phys. Acta **5**, 369 (1932).

[25] M. Han, J. Brant, and P. Kim, Phys. Rev. Lett. **104**, 056801 (2010).

[26] M. Büttiker, Y. Imry, R. Landauer, and S. Pinhas, Phys. Rev. B **31**, 6207 (1985).

[27] V. Krueckl and K. Richter, Phys. Rev. Lett. **107**, 086803 (2011).